Chinese Chemical Letters 32 (2021) 2179–2182

Contents lists available at ScienceDirect

Chinese Chemical Letters

journal homepage: www.elsevier.com/locate/cclet

Communication

In-situ construction of Z-scheme g-C_3N_4/WO_3 composite with enhanced visible-light responsive performance for nitenpyram degradation

Shiqiao Zhou[1], Ye Wang[1], Kun Zhou, Dongyang Ba, Yanhui Ao*, Peifang Wang

Key Laboratory of Integrated Regulation and Resource Development on Shallow Lakes of Ministry of Education, College of Environment, Hohai University, Nanjing 210098, China

ARTICLE INFO

Article history:
Received 10 August 2020
Received in revised form 28 October 2020
Accepted 15 November 2020
Available online 4 December 2020

Keywords:
Photocatalysis
Z-scheme
Nitenpyram
Photogenerated carriers
Environmental remediation

ABSTRACT

Developing an excellent photocatalysis system to remove pesticides from water is an urgent problem in current environment purification field. Herein, a Z-scheme WO_3/g-C_3N_4 photocatalyst was prepared by a facile in-situ calcination method, and the photocatalytic activity was investigated for degradation of nitenpyram (NTP) under visible light. The optimal Z-scheme WO_3/g-C_3N_4 photocatalyst displayed the highest rate constant (0.036 min^{-1}), which is about 1.7 and 25 times higher than that of pure g-C_3N_4 and WO_3, respectively. The improvement of photocatalytic performance is attributed to fast transfer of photogenerated carriers in the Z-scheme structure, which are testified by electron spin resonance (ESR) experiments, photocurrent and electrochemical impedance spectra (EIS) measurements. Moreover, the effects of typical water environmental factors on the degradation NTP were systematically studied. And the possible degradation pathways of NTP were deduced by the intermediates detected by high-performance liquid chromatography-mass spectrometry (HPLC-MS). This work will not only contribute to understand the degradation mechanism of pesticides in real water environmental condition, but also promote the development of new technologies for pesticide pollution control as well as environmental remediation.

Pesticide, brought agriculture to a new milestone, has kept a large variety of crops and products away from disease and insect pests, promoting the development of society to some extent [1]. Yet, in long-term pesticide abuse situations, the harmful substances in the environment have greatly increased, which have led to adverse consequences for the biosphere [2]. Most recently, nitenpyram (NTP) have been extensively used in agricultural industry by virtue of their high insecticidal activity, and wide spectrum [3]. However, the NTP is difficult to remove by water self-purification and simultaneously retain a high residue rate, which has an extremely detrimental effect on the ecological environment and human health [4,5]. Concerning the serious pollution of NTP in actual water, many strategies, such as physical adsorption, electrocatalysis, and low temperature plasma treatment, have been adopted to address the problem [6–8]. Compared with those methods, photocatalysis has intrigued much attention due to its environmental benignity and high-efficiency [9,10]. Currently, only a few literatures have reported photocatalytic degradation of neonicotinoid pesticides leveraging semiconductor materials, which only can use ultraviolet light that accounts for 5% of the sunlight [11–16]. To develop low energy pesticide removal technology, it is thus highly imperative to explore photocatalytic materials that can efficiently utilize visible light.

As a kind of metal-free polymer semiconductor, graphite carbon nitride (g-C_3N_4) is sought-after and considered to be a rather promising visible-light-responsive photocatalyst with a band gap of −2.7 eV [17–20]. Nevertheless, the challenging issue facing g-C_3N_4 is still low migration rate of charge carriers, which is restrict the practical application [21–23]. To overcome kinetic limitations and prevent the recombination of photogenerated electron-hole pairs, the construction of heterojunction shows great potential [24–26]. In traditional heterostructures, the photoinduced electrons migrate from more negative CB potential to another CB potential and holes from more positive VB potential migrate to another VB potential [27]. As a result, the holes and electrons are spatially separated, which greatly impedes their recombination [28]. However, the demerit is that the redox ability of photoexcited

* Corresponding author.
E-mail address: andyao@hhu.edu.cn (Y. Ao).
[1] The two authors contributed equally to this work.

https://doi.org/10.1016/j.cclet.2020.12.002
1001-8417/

electrons and holes is weakened after charge transfer. In sharp contrast to traditional g-C_3N_4-based heterostructure, Z-scheme photocatalysts inherit the nature photosynthesis virtues, *i.e.*, possessing the strong reducibility of g-C_3N_4, and the giant enhancement of photogenerated charge carriers separation efficiency at the same time [29,30]. In recently, a large number of g-C_3N_4-based Z-scheme heterojunction have been successfully established to enhance photocatalytic activity [31]. For example, She *et al.* [32] reported that 2D α-Fe_2O_3/g-C_3N_4 Z- scheme catalysts presented a high H_2 evolution rate. Xia *et al.* [33] demonstrated that the Z-scheme g-C_3N_4/MnO_2 photocatalysts exhibited greatly enhanced photocatalytic activities for phenol removal and dye degradation. To the best of our knowledge, the use of g-C_3N_4-based Z-scheme photocatalyst materials (especially materials with visible light activity) to remove neonicotinoids in water is still relatively rare, and the influence of water environmental factors on the activity is rarely mentioned. Additionally, the *in-situ* growth technology in the composites system can assist in forming tight contact interface, which is more favorable for the transmission of photoinduced carriers.

Bearing the aforementioned discussion in mind, it is rather more promising to explore the reasonable design and controllable preparation of efficient Z-scheme photocatalyst, and ulteriorly obtain in-depth study on NTP degradation performance and mechanism in the actual water body. In this work, Z-scheme WO_3/g-C_3N_4 photocatalyst was synthesized by *in situ* calcination approach. The degradation of NTP was utilized to evaluate the photocatalytic performance of WO_3/g-C_3N_4 under visible light irradiation. Compared with pure WO_3 and g-C_3N_4, the prepared Z-scheme WO_3/g-C_3N_4 composite photocatalyst has higher photocatalytic efficiency. The structure, morphology, optical and photoelectrochemical properties of the prepared Z-scheme composite photocatalyst was tested by various characterization methods, and its catalytic mechanism was further discussed.

Fig. 1a shows the overall synthetic process of WO_3/g-C_3N_4 sample, the specific prepartion process is in the Supporting information. The morphology of samples was studied by transmission electron microscopy (TEM). As shown in Figs. 1b and c, the clear laminar structure is observed for WO_3 sample. Fig. 1d depicts the clear and obvious lattice figure of WO_3, and the lattice spacing for 0.374 nm is consistent with the (020) crystal plane of WO_3. It can be observed from Figs. 1e and f that the flexible nanosheet with large transverse size is very thick, which is a typical feature of g-C_3N_4 nanosheets. Visually, the WO_3 has grown successfully on the surface of g-C_3N_4 nanosheets. Moreover, there is a clear tight contact interface between WO_3 and g-C_3N_4 in Fig. 1g. This interface structure is very conducive to charge carriers transmission between WO_3 and g-C_3N_4. In addition, the corresponding Transmission Electron Microscope (TEM) elemental mapping analysis was employed to indicate the composition and distribution of different components in the composite. As exhibited in Fig. 1h, C, N, O and W elements distribut homogeneous in the CW-3. Finally, the morphology of samples, in combination with XRD (Fig. S1 in Supporting information) and FT-IR (Fig. S2 in Supporting information) anlysis, collectively reveal the successful construction of WO_3/g-C_3N_4 composites.

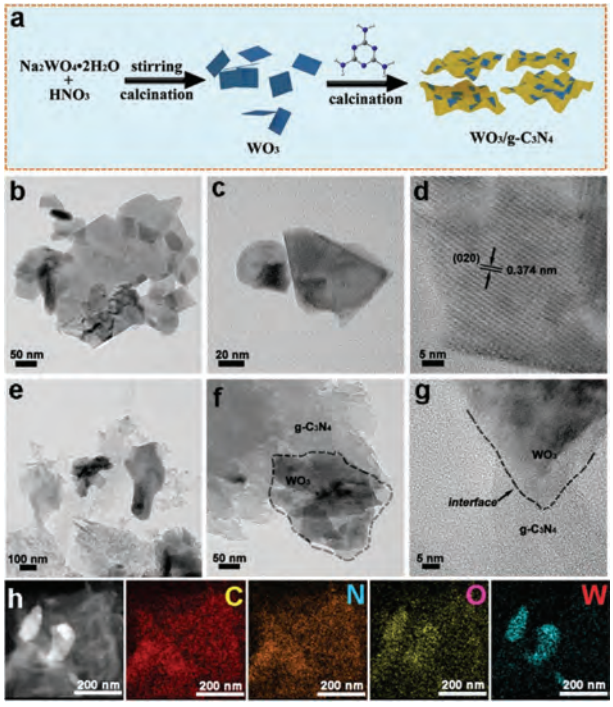

Fig. 1. Schematic illustration of the synthesis of WO_3/g-C_3N_4 nanocomposites (a), TEM images of WO_3 (b-d) and CW-3 (e-g) and TEM elemental mapping images (h) of CW-3.

As shown in Fig. 2a, the degradation efficiency of g-C_3N_4 sample was up to 51% after 30 min irradiation, and WO_3 had no degradation effect on NTP. There is no doubt that the recombination rate of photogenerated electron-hole pairs is very fast for pure semiconductor, so it exhibits relatively lower activity. The composite samples have shown enhanced photocatalytic degradation efficiency with low proportion of WO_3, while the efficiency decreased at high proportion. It can be seen that the photocatalytic degradation efficiency could achieve 68% for CW-3. Ulteriorly, the kinetics reaction constant are obtained by a *pseudo*-first-order kinetics model as follows (Eq. 1):

$$\ln(C/C_0) = -kt \quad (1)$$

where C_0 represents the initial concentration of NTP and C refers to the concentration at different irradiation times t, and k is the reaction rate constant [34]. An obvious volcano-type trend between different proportions samples and the reaction rate constant k is observed (Fig. 2b). The reaction rate constant k of CW-3 nanocomposite was 0.036 min^{-1}, which was ~1.7 and ~25 times higher than those of g-C_3N_4 and WO_3, respectively. Therefore, it is reasonable to believe that there is heterojunction interface between g-C_3N_4 and WO_3, which contribute to the improvement of photocatalytic performance. Simultaneously, as

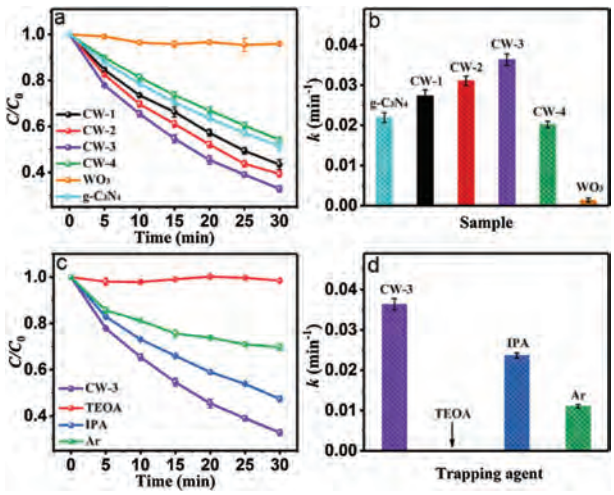

Fig. 2. The photocatalytic degradation performance of WO_3/g-C_3N_4 composites with different content of WO_3 (a); the reaction rate constant with different sample (b); capture experiment of CW-3 for NTP degradation (c) and the reaction rate constant with trapping agent (d).

presented in Figs. 2c and d, the capture experiment result indicates that h^+ and $^{\bullet}O_2^-$ act as main active substances in the experiment. Given the complexity in the water, the different type of water and the inorganic salts were employed to figure out the effect for the photocatalytic degradation of NTP from simulation experiment. It is clearly observed in Fig. S3 (Supporting information) that the different type of water and the inorganic salts have little effect on the removal of NTP, indicating that the CW-3 have good universality for NTP removal in actual water body. In addition, the pilot process and products analysis can contribute to understand the overall pathway for degradation of NTP, as shown in Fig. S5 (Supporting information).

The X-ray photoelectron spectroscopy (XPS) analysis was used to elucidate surface composition and chemical states. From the Fig. 3a, the CW-3 hybrid showed all the expected elements, including C, N, O, and W. For the high-resolution C 1s spectrum (Fig. 3b), the two peaks at binding energies of 284.94 eV and 288.28 eV could be attributed to C—C and N—C=N [35]. As shown in Fig. 3c, three peaks at 398.64 eV, 399.37 eV and 400.78 eV, can be attributed to C—N = C, N-$(C)_3$ and C=N—H, respectively, and the small peak at about 404.52 eV is caused by π excitation [36]. For the O 1s spectrum (Fig. 3d), the strong main peak at a binding energy of 530.23 eV belongs to the oxygen atom that forms the strong W—O bond, equal to the lattice O atoms of WO_3, while the weak shoulder peak at 531.34 eV can be assigned to the terminal hydroxyl groups (OH^-) on surface. Additionaly, from the O 1s spectrum of the CW-3 heterostructure, the peaks at 530.81 and 532.23 eV are assigned to the oxygen atoms in g-C_3N_4, due to the oxidation effect during thermal condensation [37]. For the high-resolution W4f spectrum (Fig. 3e), the two peaks at binding energies of 35.68 eV and 37.83 eV could be attributed to W $4f_{7/2}$ and W $4f_{5/2}$ [38]. Interestingly, compared with the pure g-C_3N_4, the peaks of C 1s and N 1s in the CW-3 heterostructure move towards higher binding energy. On the contrary, it is noted that W 4f peaks in CW-3 heterostructure shift to lower binding energy in comparison with WO_3. This demonstrates that WO_3 have a strong chemical interaction with g-C_3N_4, in favor of improving separation of charge carriers, thus enhancement of photocatalytic degradation NTP performance [39].

Electron spin resonance (ESR) experiments were performed to directly detect short-lived active species in the photocatalytic experiment [40]. As illustrated in Fig. 4a, it is very reliably to research the utility of 2,2,6,6-tetramethylpiperidine-1-oxyl (TEMPO) to marks h^+ and the employment of 5,5-dimethyl-1-pyrroline N-oxide (DMPO) to determine $^{\bullet}O_2^-$ *in-situ* formed during photoexcitation of semiconductors. With the extension of illumination time, the signal intensity of TEMPO gradually decreased, which is ascribed to the oxidation of TEMPO to $TEMPO^+$ *via* h^+ with strong oxidizing power. However, the increasing characteristic bands can be assigned to DMPO-$^{\bullet}O_2^-$ adducts for DMPO. It is clearly shown in Figs. 4b and c that the obtained CW-3 samples can produce more photogenerated carriers with the extension of illumination time, which is important for the photocatalytic reaction. Compared with the CW-3, owing to the fast recombination of charge carriers, the h^+ and $^{\bullet}O_2^-$ signals of pure sample are severely inhibited (Figs. 4d and e). In addition, Photoluminescence spectroscopy (PL) spectra (Fig. S4a in Supporting information), photocurrent (Fig. S4b in Supporting information) and electrochemical impedance spectra (EIS) plots (Fig. S4c in Supporting information) were preformed to verify that the CW-3 composite has lower electron-hole recombination rate and more efficient charge transfer. Obviously, the ESR experiments results further indicate that construction of WO_3/g-C_3N_4 heterojunction by tight connection between WO_3 and g-C_3N_4 is conducive to the separation of charge carriers, thereby enhancing the photocatalytic activity.

The above investigations included degradation activities, crystal structure, chemical environment, detailed morphological features, and charge carriers' transmission and separation. It is proposed that a heterojunction forms at the interface between g-C_3N_4 and WO_3, where accelerated electron-hole separation and improved carriers charge transfer efficiency, were witnessed by

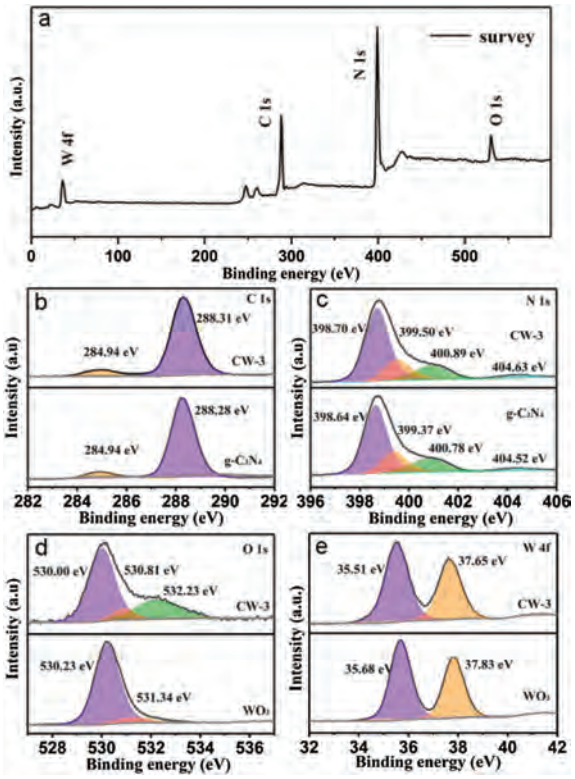

Fig. 3. The XPS survey spectra (a) and high-resolution C 1s (b), N 1s (c), O 1s (d) and W 4f (e) spectra of CW-3.

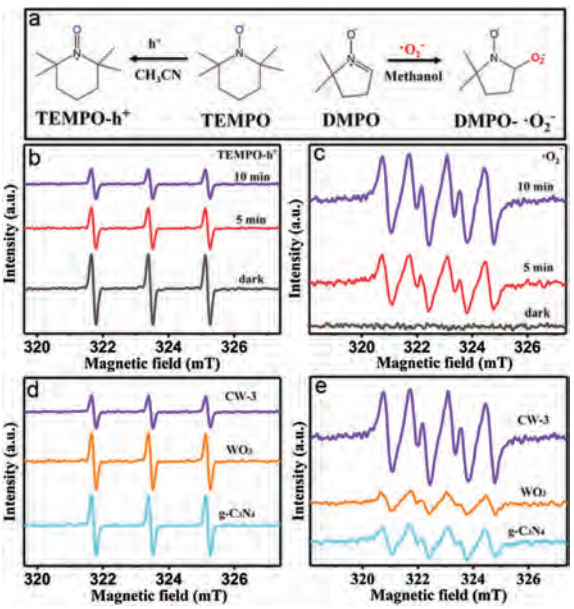

Fig. 4. Spin-trapping mechanism of TEMPO and DMPO (a); ESR signal of TEMPO radical reacting with photogenerated holes in acetonitrile dispersion of CW-3 (b); ESR signal of DMPO-$^{\bullet}O_2$ adducts in methanol dispersion over CW-3 (c); ESR signal of TEMPO radical (d) and DMPO-$^{\bullet}O_2$ adducts of as-prepared different samples (e).

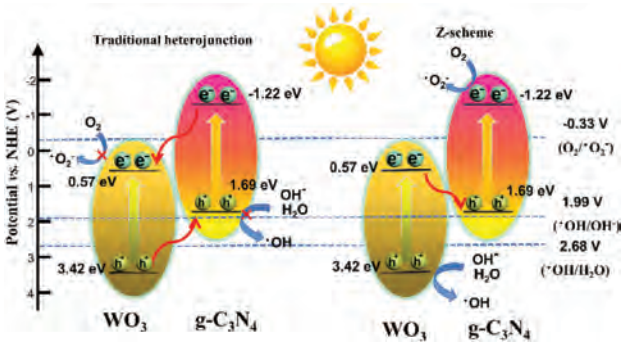

Fig. 5. Scheme diagram of proposed possible photocatalytic mechanism of CW-3.

these evidence. Based on the analysis of UV–vis DRS (Fig. S4d), both traditional heterojunction and Z-scheme mechanism may be involved for the constructed WO_3/g-C_3N_4 heterojunction materials, as shown in Fig. 5. According to the above capture experimental results and ESR analysis, the possible Z-scheme WO_3/g-C_3N_4 heterojunction degradation mechanism is suggested. In such Z-scheme heterojunction photocatalysts, photogenerated electrons accumulated on the CB position of WO_3 are more likely to recombine with the holes from the VB position of g-C_3N_4. Simultaneously, positively charge holes that remained in the VB position of WO_3 demonstrate strong oxidizing power toward photocatalytic degradation NTP, while the electrons kept on the CB position of g-C_3N_4 enable the occurrence of reduction reaction.

To sum up, Z-scheme WO_3/g-C_3N_4 photocatalyst was synthesized by *in-situ* calcination approach. The hybrids show improvement of photocatalytic activity for the degradation NTP compared with the pure sample, and the CW-3 heterostructure possess the highest photocatalytic activity. The rate constant value for NTP degradation over the Z-scheme CW-3 heterojunction is 0.036 min^{-1}, which is about 1.7 and 25 times higher than that of pure g-C_3N_4 and WO_3, respectively. The excellent photocatalytic degradation activity mainly attributes to tight heterojunction interface in the CW-3 Z-scheme structure and fast transfer of photogenerated carriers. The capture experiment and ESR results demonstrate that h^+ and $^{\bullet}O_2^-$ as main active species play the important roles in degradation of NTP. It may provide advanced insights into the construction of Z-scheme heterojunctions for effective pesticide removal in environment systems.

Declaration of competing interest

The authors declare that they have no known competing financial interests or personal relationships that could have appeared to influence the work reported in this paper.

Acknowledgments

This work was financially supported by the National Science Funds for Creative Research Groups of China (No. 51421006), National Natural Science Foundation of China (No. 51679063), the Key Program of National Natural Science Foundation of China (No. 91647206), the National key Plan for Research and Development of China (No. 2016YFC0502203), and A Project Funded by the Priority Academic Program Development of Jiangsu Higher Education Institutions (No. 51479064).

Appendix A. Supplementary data

Supplementary material related to this article can be found, in the online version, at doi:https://doi.org/10.1016/j.cclet.2020.12.002.

References

[1] A.M. Chara-Serna, L.B. Epele, C.A. Morrissey, et al., Sci. Total Environ. 692 (2019) 1291–1303.
[2] M. Samy, M.G. Ibrahim, M.G. Alalm, et al., Chem. Eng. J. 395 (2020) 124974.
[3] M.L. Tang, Y.H. Ao, C. Wang, et al., Appl. Catal. B: Environ. 270 (2020) 118918.
[4] X. Liu, C.S. Li, B.J. Zhang, et al., Chemosphere 253 (2020) 126672.
[5] T. Hirano, S. Minagawa, Y. Furusawa, et al., Toxicol Appl Pharm 383 (2019) 114777.
[6] F.Y. Suo, X.W. You, Y.Q. Ma, et al., Chemosphere 235 (2019) 918–925.
[7] Y.J. Sun, S.C. Zhu, W.Q. Sun, et al., J. Environ. Chem. Eng. 7 (2019) 103276.
[8] Y.L. Wang, L. Xu, H. Zhu, et al., Anal Methods-UK 11 (2019) 5421–5430.
[9] H.X. Zhang, Q.L. Hong, J. Li, et al., Angew. Chem. Int. Ed. 58 (2019) 11752–11756.
[10] P.Y. Kuang, P.X. Zheng, Z.Q. Liu, et al., Small 12 (2016) 6735–6744.
[11] R. Fiorenza, A. Di Mauro, M. Cantarella, et al., Chem. Eng. J. 379 (2020) 122309.
[12] T.X. Xu, J.P. Wang, Y. Cong, et al., Chin. Chem. Lett. 31 (2020) 1022–1025.
[13] P.L. Ji, X.Z. Kong, J.G. Wang, et al., Chin. Chem. Lett. 23 (2012) 1399–1402.
[14] M. Wang, Y.X. Liu, D. Li, et al., Chin. Chem. Lett. 30 (2019) 985–988.
[15] M.B. Kralj, E.G. Dilcan, G. Salihoglu, et al., J. Anal. Chem. 74 (2019) 1371–1377.
[16] Z.P. Yan, W.C. Wang, L.L. Du, et al., Appl. Catal. B: Environ. 275 (2020) 119151.
[17] X.H. Wu, D.D. Gao, P. Wang, et al., Carbon 153 (2019) 757–766.
[18] M.L. Tang, Y.H. Ao, C. Wang, et al., Appl. Catal. B: Environ. 268 (2020) 118395.
[19] K.L. He, J. Xie, Z.Q. Liu, et al., J. Mater. Chem. A 6 (2018) 13110–13122.
[20] X. Zhang, X.Z. Yuan, L.B. Jiang, et al., Chem. Eng. J. 390 (2020) 124475.
[21] X.H. Wu, H.Q. Ma, W. Zhong, et al., Appl. Catal. B: Environ. 271 (2020) 118899.
[22] Y.H. Wu, Q. Chen, S. Liu, et al., Chin. Chem. Lett. 30 (2019) 2186–2190.
[23] J.X. Huang, D.G. Li, R.B. Li, et al., J. Hazard. Mater. 386 (2020) 121634.
[24] R.H. Mu, Y.H. Ao, T.F. Wu, et al., J. Hazard. Mater. 382 (2020) 121083.
[25] A. Beyhaqi, Q.Y. Zeng, S. Chang, et al., Chemosphere 247 (2020) 125784.
[26] M.X. Liang, Z.S. Zhang, R. Long, et al., Environ. Pollut. 259 (2020) 113770.
[27] N.C. Zheng, T. Ouyang, Y.B. Chen, et al., Catal. Sci. Technol. 9 (2019) 1357–1364.
[28] J.X. Low, J.G. Yu, M. Jaroniec, et al., Adv. Mater. 29 (2017) 1601694.
[29] P. Zhou, J.G. Yu, M. Jaroniec, et al., Adv. Mater. 26 (2014) 4920–4935.
[30] Y.K. Sun, Q. Zhu, B. Bai, et al., Chem. Eng. J. 390 (2020) 124518.
[31] M. Ding, J.J. Zhou, H.C. Yang, et al., Chin. Chem. Lett. 31 (2020) 71–76.
[32] X.J. She, J.J. Wu, H. Xu, et al., Adv. Energy Mater. 7 (2017) 1700025.
[33] P.F. Xia, B.C. Zhu, B. Cheng, et al., ACS Sustain. Chem. Eng. 6 (2018) 965–973.
[34] Y.H. Fu, W. Liang, J.Q. Guo, et al., Appl. Surf. Sci. 430 (2018) 234–242.
[35] J.H. Ge, L. Zhang, J. Xu, et al., Chin. Chem. Lett. 31 (2020) 792–796.
[36] C.X. Zhao, Z.P. Chen, J.S. Xu, et al., Appl. Catal. B: Environ. 256 (2019) 117867.
[37] W.L. Yu, J.X. Chen, T.T. Shang, et al., Appl. Catal. B: Environ. 219 (2017) 693–704.
[38] J.W. Fu, Q.L. Xu, J.X. Low, et al., Appl. Catal. B: Environ. 243 (2019) 556–565.
[39] Q.L. Xu, B.C. Zhu, C.J. Jiang, et al., Sol. RRL. 2 (2018) 1800006.
[40] X.F. Yang, L. Tian, X.L. Zhao, et al., Appl. Catal. B: Environ. 244 (2019) 240–249.